EVALUATION OF RESIDENCE TIME DISTRIBUTION FOR BUBBLE TRAIN FLOW IN A SQUARE MINI-CHANNEL BY DIRECT NUMERICAL SIMULATION

Martin Wörner[*], Bradut Ghidersa, Alexandru Onea

Forschungszentrum Karlsruhe, Institut für Reaktorsicherheit, Postfach 3640, 76021 Karlsruhe, Germany
[*] Email: woerner@irs.fzk.de, Phone: +49 7247 82 2577

ABSTRACT

This paper presents an original method for evaluating the liquid phase residence time distribution in bubble train flow using data from direct numerical simulations. The method is a particle method and relies on the uniform introduction of virtual particles in the volume occupied by the liquid phase within a single flow unit cell. The residence time distribution for such a volumetric introduction is obtained by statistical evaluation of the time needed by any particle to travel an axial distance equivalent to the length of the flow unit cell. Residence time curves are evaluated from DNS data of bubble train flow in a square mini-channel for different length of the flow unit cell. The curves obtained can well be fitted by a simple exponential relationship. The latter has been developed on the basis of a compartment model which consists of two tanks in series, the first tank being a plug flow reactor and the second being a perfectly stirred vessel. It is argued that the model derived may also be a good representation for the real liquid phase residence time distribution in bubble train flow with flux introduction and measurement.

1   INTRODUCTION

Bubble train flow (BTF) is a common flow pattern for gas-liquid flows in narrow channels. It consists of a regular sequence of bubbles of identical shape which fill almost the entire channel cross-section (Taylor bubbles). The individual bubbles are separated by liquid slugs and move with the same axial velocity. Therefore, BTF is fully described by a single flow unit cell which consists of one bubble and the liquid slug separating it from the trailing bubble. BTF is of technical relevance for monolithic reactors [1], for micro-bubble columns [2] and for other miniaturized multiphase reactors involving slug flow [3].

An important characteristic of any chemical reactor is its residence time distributions (RTD), since this provides information about the flow and mixing behaviour of reaction components. In practice, the residence time distribution is often measured by a stimulus-response technique, where a specific quantity of tracer (e.g. fluorescent substance, radionuclide, solution of salt, etc.) is introduced at the system inlet as a short duration pulse or step function and where the time variation of the tracer concentration at the outflow is recorded.

The tracer particles injected at the inlet are assumed to follow the same paths through the system as did the original fluid particles they replaced [4]. Thus, the tracer particles will have the same distribution of residence times as the original fluid particles. By recording the times when particles leave, a histogram can be constructed which, with a large sampling size, will converge to the differential residence time distribution function, $E(t)$. The probability that a particle had a residence time less than t is then given by the cumulative residence time distribution function

$$F(t) = \int_0^t E(t')\mathrm{d}t' \qquad (1)$$

The extension of the above measurement principle from single phase flow to gas-liquid two phase flow presents no special difficulties [4]. The main difference is that the system now usually has two inlets (one for the gas phase and one for the liquid phase) while there is still one common outlet. To measure the residence time distribution of the liquid phase, the tracer pulse is injected at the liquid inlet only. For bubble train flow, a measurement of the residence time distribution of the gas phase is not of interest, since its mean residence time can easily be determined from the bubble velocity.

The described measurement concept is well suited for macro-reactors where the reactor volume is much larger than the volume of the tracer measuring unit. However, for micro-reactors the reactor volume is usually smaller than the volume of the measuring unit. This means that the residence time response of the tracer may already be influenced by the measuring construction itself [5]. Measurements of RTD in narrow channels are reported by Heibel et al. [6] and Yawalkar et al. [7] for the film flow in a monolith reactor and by Günther et al. [8] for bubble train flow in micro-fluidic channel networks of rectangular cross-section.

An alternative way to determine the RTD is by means of computational fluid dynamics (CFD). There exist in principle two options to determine the residence time distribution from CFD methods [9]. The first one is to numerically simulate the stimulus-response experiment, i.e. setting a short concentration pulse at the inlet of the computational domain, computing the unsteady concentration field of the tracer within the computational domain and evaluating it at the outlet. The second possibility is the particle tracking method. Here, virtual particles are released at the inlet and their trajectories are computed from the known velocity field of the CFD calculation (see e.g. [10]). A notable difference between both methods is that in evaluating the unsteady concentration field in addition to convective transport diffusive transport may be

taken into account, too, whereas in the particle method only convective properties of the flow are monitored.

An important issue when computing the RTD by CFD is the introduction of the tracer at the inlet and its detection at the outlet, because this may strongly influence the obtained residence time distribution [11]. There are essentially two different concepts, namely the flux and planar introduction and measurement, respectively. Both lead to different response curves which may, for laminar pipe flow, be transformed into each other, see section 3.2. As pointed out by Levenspiel [11], only the flux-flux method yields the proper RTD for reactor purposes. To distinguish it from the response curve obtained by a planar-planar method, we will call the latter one P-RTD.

In this paper we present an original CFD-based method for evaluation of the residence time distribution of the continuous phase for a bubble-train flow. Our method is a particle method and relies on the known bubble shape and velocity field within a unit cell, which are assumed to be available from direct numerical simulation (DNS). The particle method is usually based on the computed *steady* velocity field. For BTF the velocity field is *unsteady* in the fixed frame of reference, for which the RTD needs to be computed. It is, however, steady in the frame of reference moving with the bubble. In our method we take advantage of this fact and apply an appropriate transformation between both frames of reference. Because the concept of planar introduction is not suited for BTF, we extend it to a "volumetric introduction", where virtual particles are introduced in all mesh cells within the flow domain that are entirely filled with liquid. For each particle we determine the time the particle needs to travel an axial distance equal to the unit cell length. By normalizing the resulting histogram we obtain a residence time curve which we call V-RTD.

The remainder of this paper is organized as follows. In section 2 we present the direct numerical simulations, where we consider the co-current upward flow of air bubbles through silicon oil in a square vertical channel with a cross section of 2 mm × 2 mm. In section 3 we introduce our original particle method for evaluating the V-RTD for bubble train flow. In section 4 we present results for the V-RTD curve of the liquid phase in bubble train flow. Finally, we give conclusions and outlook in section 5.

2 DNS OF BUBBLE TRAIN FLOW

In this section we give a short overview on the numerical method and the computer code used to compute bubble train flow and then discuss the results obtained by previous direct numerical simulations of BTF.

2.1 Numerical method

The DNS are performed with the in-house computer code TURBIT-VOF which solves the Navier-Stokes equations with surface tension term in single-field formulation for two incompressible immiscible fluids under assumption of constant fluid properties (density, viscosity, surface tension). The governing equations are written in non-dimensional form, see [12], where for normalization a reference length L_{ref} and reference velocity U_{ref} are used, which both need to be specified. The solution strategy is based on a projection method, where the resulting Poisson equation for the pressure is solved by a conjugate gradient solver. Time integration of the single field Navier-Stokes equation is done by an explicit third order Runge-Kutta method. Discretization in space is by a finite volume method where a regular Cartesian staggered grid

is used. All derivatives in space are approximated by second order central differences.

For computing the evolution of the deformable interface that separates the two immiscible fluids, the volume-of-fluid (VOF) method is used. As an approximation, we locally represent the interface in any mesh cell that instantaneously contains both phases by a plane. The orientation and location of the plane is reconstructed from the discrete distribution of the volumetric fraction f of the continuous fluid. Note that $f = 1$ for mesh cells entirely filled with liquid, $f = 0$ for mesh cells entirely filled with gas, and $0 < f < 1$ for mesh cells instantaneously containing both fluids. The evolution of f is governed by an advection equation which expressed the mass conservation of the continuous phase. To avoid any smearing of the interface, this f-equation is not solved by a difference scheme. Instead, the flux of f across the faces of any interface mesh cell is calculated in a geometrical manner, depending on the location and orientation of the interface representing plane. For further details about the numerical method we refer to [13].

2.2 Simulations of bubble train flow

We now give a short overview on the previously performed simulations of bubble train flow (see [12] and [14]) that we use here to analyse the RTD. The bubble train flow simulations consider one flow unit cell only and use periodic boundary conditions in vertical axial direction (y). Otherwise, the simulations reproduce the conditions of an experiment by Thulasidas et al. [15], where the co-current upward flow of air bubbles in silicon oil of various viscosities in a square vertical channel with a cross section of 2 mm × 2 mm is investigated. Simulations were performed for silicon oil with two different viscosities, which results in different values of the capillary number $Ca = \mu_l U_B / \sigma$, namely $Ca \approx 0.04$ and $Ca \approx 0.2$. The capillary number is the relevant non-dimensional group for two-phase flow in narrow channels, as it represents the ratio of the two dominant forces, namely viscous forces and surface tension. The influence of the capillary number is discussed in detail in [12]. In the present paper, we consider only the more viscous case, i.e. that with higher value of Ca, where $\mu_l = 0.048$ Pa s and $\rho_l = 957$ kg/m^3. While these values for density and viscosity match the experiment of Thulasidas et al. [15], we increased the gas density and gas viscosity by a factor of 10 to improve the computational efficiency. So we use $\mu_g = 1.48 \times 10^{-4}$ Pa s and $\rho_g = 11.7$ kg/m^3 while the coefficient of surface tension is the same as in [15], i.e. $\sigma = 0.02218$ N/m.

For the above physical parameters a detailed study of the influence of the length of the flow unit cell has been performed by a series of five simulation runs, see [14]. Using $L_{ref} = 2$ mm, the computation domain is a box of non-dimensional size $L_x \times L_{uc} \times 1$. Here, a square channel is considered so that $L_x = 1$. The non-dimensional length of the flow unit cell L_{uc} is varied from 1 for case A to 2 for case E, see Table 1. To test whether the resolution of 48 mesh cells per unit length is sufficient, a grid refinement study has been performed for case A. The comparison of the results obtained with the 48 × 48 × 48 grid with those of an additional simulation with a grid consisting of 64 × 64 × 64 mesh cells showed only very small differences. Therefore the simulations of case B – E have been performed with the coarser resolution. Table 1 lists the grid parameters of the different runs. In all five cases the gas content in the computational domain is $\varepsilon = 33\%$ and the same driving axial pressure gradient is applied in y-direction, which is the direction of flow. For each case about 50,000 time steps of

(non-dimensional) width $\Delta t = 2.5 \cdot 10^{-5}$ are computed till the non-dimensional bubble velocity U_B and the non-dimensional mean liquid velocity U_L (both scaled by $U_{ref} = 26.4$ mm/s) reached steady values. From the respective data listed in Table 1 we see, that with the increase of the length of the flow unit cell both, U_B and U_L increase, too.

Table 1: Direct numerical simulations of bubble train flow

Case	L_{uc}	domain	grid	U_B	U_L
A	1	1×1×1	48×48×48	3.60	1.21
B	1.25	1×1.25×1	48×60×48	3.61	1.29
C	1.5	1×1.5×1	48×72×48	3.83	1.37
D	1.75	1×1.75×1	48×84×48	4.17	1.44
E	2	1×2×1	48×96×48	4.50	1.51

For verification of the simulation runs a comparison with experimental results of Thulasidas et al. [15] is performed. As shown in [14] we obtained good agreement for the bubble diameter, the bubble velocity normalized by the total superficial velocity, and for the relative velocity between bubble and liquid slug scaled by the total superficial velocity.

Figure 1 shows a visualization of the computed bubble shape and flow field for the five cases. To allow for a good visualization, the results are shown for each case for an instant in time when the bubble tip is almost at the top of the computational domain. In all five cases the bubble is axisymmetric, i.e. its cross section at any axial position is circular. It is therefore sufficient to display only the left half of the steady bubble shape.

Figure 1 also shows the velocity field in the axial mid-plane for the five cases. In the left half of the figure the velocity field is shown in the fixed frame of reference while in the right half it is displayed in the frame of reference moving with the bubble, i.e. the bubble velocity is subtracted from the vertical velocity component. In the fixed frame of reference it can be seen that the velocity profile in the liquid slug has the form of a parabola and is similar for all five cases. In the region where the liquid film is very thin the liquid velocity is almost zero. In the frame of reference moving with the bubble the flow inside the bubble can be analyzed. We find that there is one big vortex which occupies almost the complete bubble. In the rear part of the bubble, however, the velocity is almost zero in the moving frame of reference. For the flow in the liquid, the blank regions in the right half of the figures indicate that part of the liquid slug that is moving with the velocity of the bubble.

3 NUMERICAL EVALUATION OF RTD

3.1 Tracking of mass-less particles

We now describe our procedure to evaluate the V-RTD from the DNS data and start by presenting the method for the reconstruction of the tracer paths. In this context we introduce the following definitions. Let $\mathbf{x}_{p,j}$ be the position vector of particle j in the fixed frame of reference and let $\mathbf{v}(\mathbf{x},t)$ be the velocity field in the fixed frame of reference. Then, the time variation of the position of an infinitesimal small mass-less particle in the fixed frame of reference is given by

$$\frac{d\mathbf{x}_{p,j}}{dt} = \mathbf{v}\left(\mathbf{x}_{p,j}(t), t\right) \tag{2}$$

Thus, if one knows the particle position at time t^n, then the position at time $t^{n+1} = t^n + \Delta t^n$ is given by

$$\mathbf{x}_{p,j}(t^{n+1}) \equiv \mathbf{x}_{p,j}^{n+1} = \mathbf{x}_{p,j}^n + \int_{t^n}^{t^{n+1}} \mathbf{v}\left(\mathbf{x}_{p,j}(t), t\right) dt \tag{3}$$

Using an explicit first order Euler forward integration procedure, one can approximate the above formula as

$$\mathbf{x}_{p,j}^{n+1} = \mathbf{x}_{p,j}^n + \Delta t^n \cdot \mathbf{v}(\mathbf{x}_{p,j}^n, t^n) \tag{4}$$

This means to compute the new position of the tracer particle one needs to know the fluid velocity at the particles actual position. For the case of bubble-train flow the phases are in relative motion, so that the velocity field in the fixed frame of reference changes in time. However, for periodic fully developed bubble-train flow the bubbles move with constant speed $\mathbf{U}_B = (0, U_B, 0)^T$ and a steady flow is recovered in the referential linked to the centre of mass of the bubble. Let $\mathbf{z}_{p,j}$ be the position vector of particle j in the frame of reference moving with the bubble and let $\mathbf{w}(\mathbf{x})$ be the steady velocity field in this frame of reference. Then, the relation between the position vector in the moving frame of reference and in the fixed frame of reference is given by

$$\mathbf{z} = \mathbf{x} - (t - t_0)\mathbf{U}_B, \tag{5}$$

where t_0 is the time level for which both frames of reference coincide. Here we use $t_0 = 0$. At the same time, the velocity fields in the moving frame of reference and in the fixed frame of reference are related by

$$\mathbf{w}(\mathbf{z}) = \mathbf{v}(\mathbf{x}, t) - \mathbf{U}_B \tag{6}$$

Thus, in a discrete representation in time we obtain from the last two equations

$$\mathbf{z}_{p,j}^n = \mathbf{x}_{p,j}^n - t^n \mathbf{U}_B \tag{7}$$

and

$$\mathbf{v}(\mathbf{x}_{p,j}^n, t^n) = \mathbf{w}(\mathbf{z}_{p,j}^n) + \mathbf{U}_B \tag{8}$$

Inserting Eq. (8) into Eq. (4) we finally obtain

$$\mathbf{x}_{p,j}^{n+1} = \mathbf{x}_{p,j}^n + \Delta t^n \cdot \left(\mathbf{w}(\mathbf{z}_{p,j}^n) + \mathbf{U}_B\right) \tag{9}$$

Equation (9) together with Eq. (7) allow us to compute the particle path in the fixed frame of reference from knowing the steady velocity field in the moving frame of reference.

As mentioned above, our DNS computer code uses a regular rectilinear staggered grid. Thus, the components of the velocity vector are defined at the centre of those two faces of a mesh cell that are normal to the respective coordinate direction. To determine the velocity at the particle position we perform for each velocity component a linear interpolation, which involves the eight nearest face-centred values of the respective velocity component. The time step width Δt^n for the forward Euler step is determined so that the Courant number based on the local particle velocity takes a constant value (here this value is 0.1).
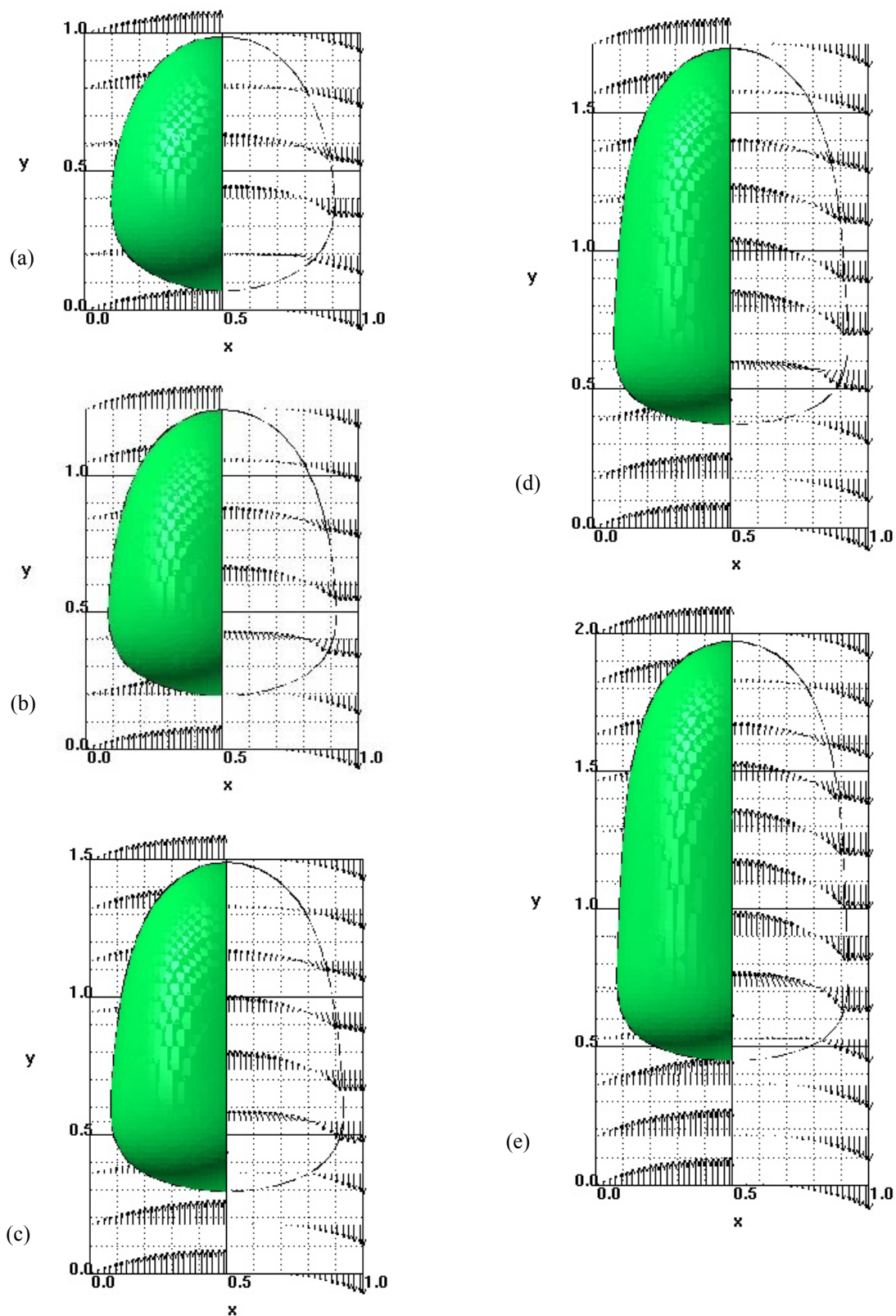
Fig. 1. Bubble shape and velocity field in plane $z = 0.5$ for fixed frame of reference (left half) and for frame of reference linked to the bubble (right half) for (a): case A, $t = 0.595$, (b): case B, $t = 0.38$, (c): case C, $t = 0.44$, (d): case D, $t = 0.51$, (e): case E, $t = 0.54$. In y-direction only every 8th vector is displayed.
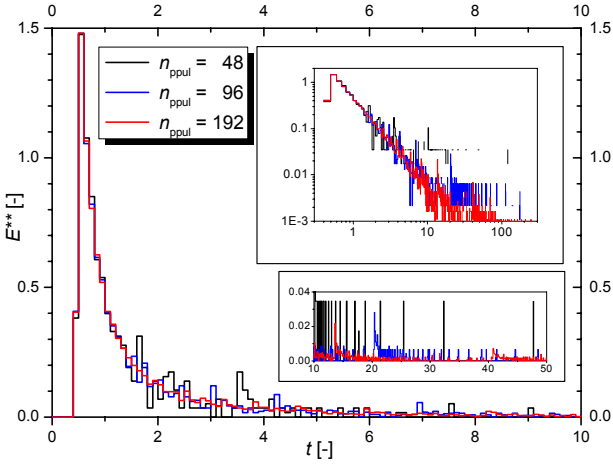
Fig. 2: Non-dimensional E^{**} curves for laminar single phase flow in a square duct for different values of n_{ppul}.
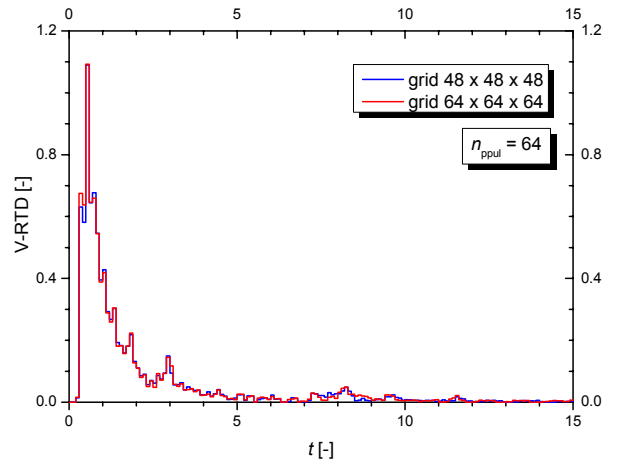
Fig. 3: Non-dimensional V-RTD curves for the bubble train flow of case A on two different grids for $n_{ppul} = 64$.

3.2 Initializing the particle positions

Up to now we have discussed only the problem of finding the position of a particle at a certain moment of time assuming that its position at a previous time step is known. In order to compute the RTD we must define the initial positions where the particles are released into the flow. Additionally, we have to define a criterion to determine when a particle has left the domain. Thus, we have to discuss the methods for introducing the numerical tracer and for "measuring" it.

Single phase flow. Levenspiel [11] points out that there exist two different ways of introducing and measuring tracer. These are the flux introduction and planar introduction and the flux measurement and planar measurement, respectively. In the flux introduction method the amount of tracer introduced within the cross-section of a duct is proportional to the velocity within this cross-section. Thus, more tracer particles are released in the centre of the duct and less close the walls, where the velocity is low. Accordingly, the principle of the flux measurement method is to catch all the exit fluid by a "mixing cup measurement". The flux introduction and flux measurement are thus related to the volumetric flow rate entering and leaving the duct within a certain time interval. In contrast, the planar introduction and planar measurement do not rely on a time interval but on a certain instant in time. Therefore, in the planar introduction the tracer is evenly distributed across the cross-section of the duct while the planar measurement detects the instantaneous tracer concentration within the cross-section.

It is important to note, that the various combinations of the input-output methods give different curves [11]. For reactor purposes, the flux introduction - flux measurement method (flux-flux) is appropriate and gives the proper RTD curve denoted as E. The flux-planar and planar-flux methods yield the curve E^* while the planar-planar method yields E^{**}. For laminar single-phase pipe flow the different curves can be transformed by the relationship

$$E^{**} = \frac{t}{\tau} E^* = \frac{t^2}{\tau^2} E = \begin{cases} 0 & \text{for} \quad t < \tau / 2 \\ \dfrac{1}{2t} & \text{for} \quad t \geq \tau / 2 \end{cases} \quad (10)$$

Here, τ is the mean hydrodynamic residence time, defined as the ratio of pipe volume V and volumetric flow rate Q

$$\tau \equiv \frac{V}{Q} \quad (11)$$

From Eq. (10) we see that the tail of E is proportional to t^{-3}, that of E^* is proportional to t^{-2} and that of E^{**} is proportional to t^{-1}. While the mean value of E is identical to τ, the mean values of E^* and E^{**} are ∞ which is a consequence of the long tails.

The flux-flux method is suitable for a CFD method where the RTD is computed by solving a convection-diffusion equation for the tracer concentration. For a particle method the realisation of the flux-flux method is not straight forward. Therefore, in the present approach we choose the planar-planar method and thus obtain E^{**} instead of E.

To test our particle method we computed the laminar single phase flow in a straight duct with square cross-section. In the simulations a cubic domain of non-dimensional size $1 \times 1 \times 1$ is used which is discretized by $48 \times 48 \times 48$ uniform mesh cells. The flow is in y-direction. In this direction periodic boundary conditions are used while at $x = z = 0$ and $x = z = 1$ no-slip conditions apply. Starting from fluid at rest, fully developed flow is obtained after some time, and the computed velocity field agrees well with the analytical solution.

In order to obtain reliable results with the planar introduction method it is essential that the particles are uniformly distributed in the inlet plane. This is ensured by specifying a certain number of particles per unit length n_{ppul}, which is an input parameter of our method. The non-dimensional distance between neighbouring particles in each coordinate direction is therefore $1 / n_{ppul}$. For a cross-section of size 1×1 then $n_{ppul} \times n_{ppul}$ particles are released in the inlet plane at $y = 0$. E.g. for $n_{ppul} = 50$ the particle positions in x and y-direction are 0.01, 0.03, 0.05, ..., 0.99. We then computed the trajectories of the $N_p = n_{ppul} \cdot n_{ppul}$ particles and stored for each particle the time needed to reach the outlet plane at $y = 1$. So, the axial distance each particle travels is $L_{travel} = 1$. By classifying the travel time of all particles in certain time intervals a histogram is produced. Here, as time interval for each class $\Delta t_{class} = 0.1$ is used. The histogram is then normalized by $n_{ppul} \cdot n_{ppul} \cdot \Delta t_{class}$ to obtain the E^{**} curve.

In Fig. 2 we show the E^{**} curves obtained for $n_{ppul} = 48$, $n_{ppul} = 96$, and $n_{ppul} = 192$. We see that the E^{**} curve has the typical shape for laminar flow. It is zero for times smaller than the breakthrough time, takes a sharp peak at about the breakthrough time and then shows a decay. For times $t < 1.5$ all three E^{**} curves agree well. However, for larger values of t

there are some discrepancies, see lower right inset graphic in Fig. 2. These discrepancies are not surprising. In fact, one may expect that a continuous E^{**} curve at large values of t requires a very fine resolution with many particles close to the wall. The upper right inset graphics in Fig. 2 shows the E^{**} curves in double logarithmic scale. In this representation, the curve for $n_{ppul} = 192$ can well be fitted by a line indicating the typical power law dependence of laminar flow.

The mean value of the E^{**} curve is 2.87 for $n_{ppul} = 48$, is 3.47 for $n_{ppul} = 96$, and is 4.13 for $n_{ppul} = 192$. These values are clearly larger than the mean hydraulic residence time which takes a value of $\tau = 1.0$. The increase of the mean value of the E^{**} curve with increasing number of particles suggests that the mean value will go to infinity for large values of n_{ppul} as it should for laminar flow.

Two-phase flow. While the planar introduction method described above is reasonable to determine the E^{**} curve for single phase flow, it can not be used for a two phase flow. The reason is that releasing particles at a certain instant in time in a cross-section fully occupied by liquid (i.e. a cross-section within the liquid slug) will not be a representative particle subset for the liquid phase. By such a procedure the contributions of the liquid film flow and the corner flow would be missed. Therefore, with exception of two-phase flows which do not show any axial variation of the cross-sectional void distribution (i.e. stratified flow and annular flow) the concept of planar introduction must be extended.

In this paper we propose an extension of the planar introduction concept from single-phase flow to two-phase flow, namely the *volumetric introduction*. To have a representative sample of particles we adopt the following procedure. With the normalization used in TURBIT-VOF the non-dimensional size of the computation domain is $L_x \times L_{uc} \times 1$ and the non-dimensional volume is $L_x L_{uc}$. Within this domain $n_{ppul} \cdot L_x \times n_{ppul} \cdot L_{uc} \times n_{ppul}$ are uniformly distributed.

The non-dimensional volume occupied by the liquid phase within the computational domain is

$$V_L = (1 - \varepsilon) L_x L_{uc} \tag{12}$$

Here, ε is the overall volume fraction of the gas phase. The number of particles in the liquid phase is thus approximately

$$N_p = (1 - \varepsilon) L_x L_{uc} n_{ppul}^3 \tag{13}$$

In practice, particles are only released in mesh cells that are entirely filled with liquid. Thus, mesh cells which contain both liquid and gas are ignored.

In our DNS simulations the flow is spatially periodic and the periodicity length is equal to the length of the flow unit cell L_{uc}. It is therefore reasonable to take the travelling distance to be a multiple of the length of the flow unit cell

$$L_{travel} = n_{uc} L_{uc} \tag{14}$$

Here, n_{uc} is a positive integer. In this paper we will only consider the case $n_{uc} = 1$.

4. RESULTS FOR BUBBLE TRAIN FLOW

In this section we give results for the non-dimensional V-RTD curve of the liquid phase in bubble train flow. To test the accuracy and grid sensitivity of the method we first apply it to the two simulations performed for case A with a grid consisting of $48 \times 48 \times 48$ mesh cells and $64 \times 64 \times 64$ mesh cells, respectively. For this comparison we use $n_{ppul} = 64$. The results are displayed in Fig. 3. They show that the V-RTD computed from both DNS data sets is quite similar. Note that in this and all other figures the time is dimensionless, at it is normalized by $t_{ref} \equiv L_{ref} / U_{ref} = 75.76$ ms.

In Fig. 4 we show the V-RTD curve for BTF case A on grid $48 \times 48 \times 48$ for three different values of n_{ppul}. While the curves are very similar, that one for $n_{ppul} = 96$ is clearly the smoothest especially for larger values of t. The inset graphics in Fig. 4 shows the curve for $n_{ppul} = 96$ in semi-logarithmic representation. The constant slope indicates that the curve may well be approximated by an exponential relationship. Also shown in Fig. 4 as dashed vertical line is the non-dimensional bubble breakthrough time

$$t_B \equiv \frac{L_{uc}}{U_B} \tag{15}$$

This is the time the bubble needs to move an axial distance of $L_{travel} = L_{uc}$. From Fig. 4 we see that no fluid particles are moving faster then the bubble, a result that was expected. However, most of the fluid particles have a residence time that is only slightly larger than t_B. These fluid particles belong to the liquid slug region behind the bubble, which is moving almost with the bubble velocity, as indicated by the velocity profiles in the right half of Fig. 1. The long tails in the V-RTD on the other hand correspond to the flow in the liquid film which is almost stagnant (see velocity profiles in the left half of Fig. 1).

The shape of the V-RTD curve in Fig. 4 suggests that if it would be the real RTD it could well be approximated by a compartment model consisting of two tanks in series, where the first "tank" is a plug flow reactor and the second "tank" is a perfectly stirred vessel (see Fig. 12.1 in [11]). We therefore propose the following approximation for the V-RTD curve

$$E_{VRTD} = \begin{cases} 0 & \text{for } t < L_{uc} / U_B \\ \dfrac{U_L}{L_{uc}} \exp\left(-\dfrac{U_L}{L_{uc}} \cdot t + \dfrac{U_L}{U_B} \right) & \text{for } t \geq L_{uc} / U_B \end{cases} \tag{16}$$

and as an alternative

$$E_{VRTD} = \begin{cases} 0 & \text{for } t < L_{uc} / U_B \\ \dfrac{J_L}{L_{uc}} \exp\left(-\dfrac{J_L}{L_{uc}} \cdot t + \dfrac{J_L}{U_B} \right) & \text{for } t \geq L_{uc} / U_B \end{cases} \tag{17}$$

where we replace the mean liquid velocity U_L by the liquid superficial velocity $J_L \equiv (1 - \varepsilon) U_L$.

Note that in above formulas the inverse of the pre-factor of the exponential term defines the mean residence time of the perfectly stirred tank. With A_{cs} as the cross-sectional area of the duct, the volume of the unit cell is given by $V = L_{uc} \cdot A_{cs}$ while the liquid volumetric flow rate is $Q = J_L \cdot A_{cs.}$. Equation (11) thus gives a mean residence time of $V / Q = L_{uc} / J_L$ which indicates that Eq. (17) might be the better model.
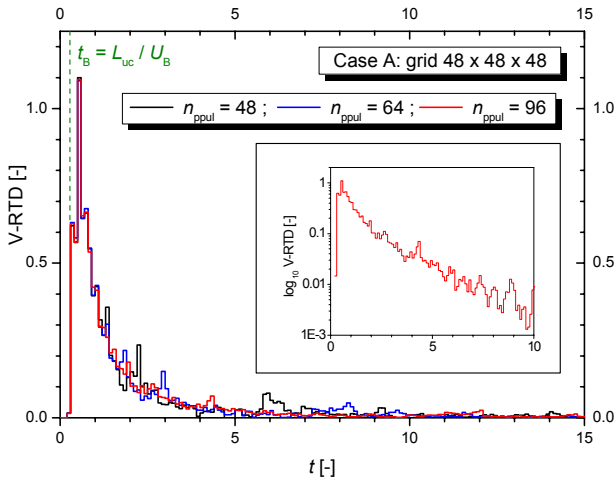
Fig. 4: Computed V-RTD curves for BTF case A (grid 48 × 48 × 48) for three different values of n_{ppul}. The inset figure shows the curve for $n_{ppul} = 96$ in semi-logarithmic scale. The dashed green line indicates the bubble breakthrough time.
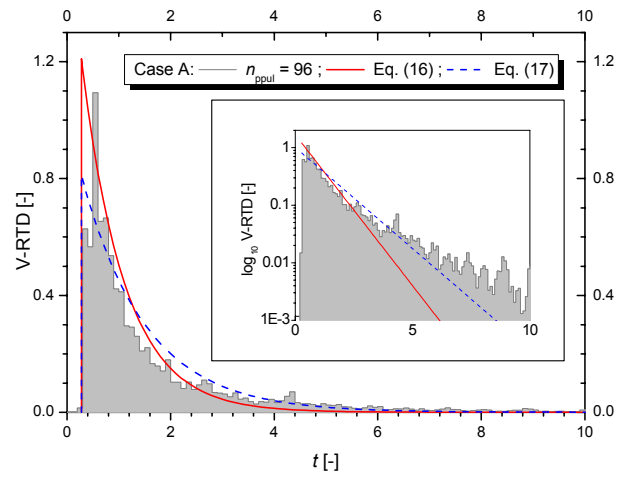
Fig. 5: Comparison of evaluated V-RTD for BTF case A (grid 48 × 48 × 48) and $n_{ppul} = 96$ with model equations (16) and (17).
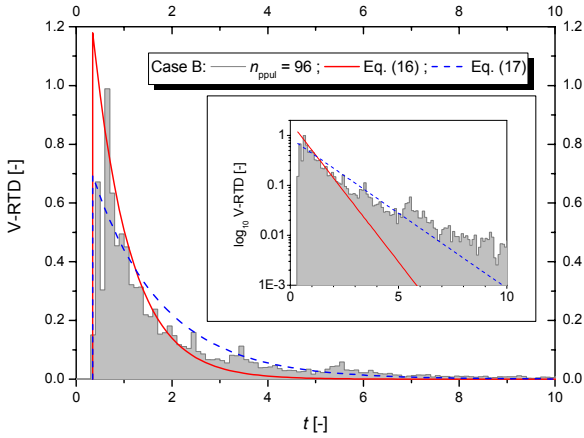
Fig. 6: Comparison of evaluated V-RTD for BTF case B and $n_{ppul} = 96$ with model equations (16) and (17).
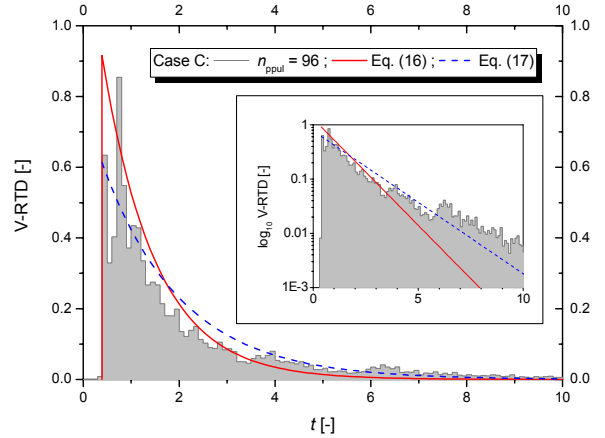
Fig. 7: Comparison of evaluated V-RTD for BTF case C and $n_{ppul} = 96$ with model equations (16) and (17).
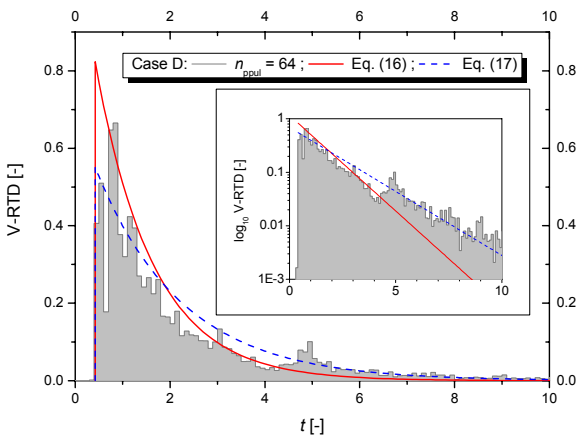
Fig. 8: Comparison of evaluated V-RTD for BTF case D and $n_{ppul} = 64$ with model equations (16) and (17).
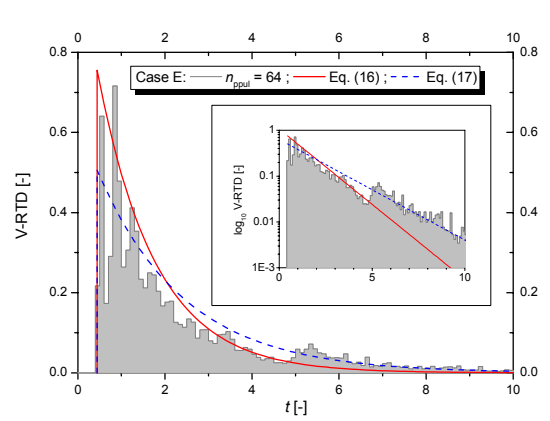
Fig. 9: Comparison of evaluated V-RTD for BTF case E and $n_{ppul} = 64$ with model equations (16) and (17).

In Figures 5 to 9 we compare the model equations (16) and (17) with the evaluated V-RTD curves for cases A to E. In all these figures the data are represented in the main graphics as linear plot and in the inset graphics as semi-logarithmic plot. In the linear plots we see that the peak value clearly decreases as the length of the flow unit cell increases from $L_{uc} = 1$ in case A to $L_{uc} = 2$ in case E. Therefore, for larger values of L_{uc} the tails in the V-RTD become more important. The evaluated V-RTD curves themselves are not very smooth, indicating that a larger value of n_{ppul} might be used. Nevertheless, in the semi-logarithmic plots one can recognize that for $t \approx 4 - 5$ the curves change their slope. The steeper slope for lower values of t is well fitted by model equation (16) while the flatter slope for larger values of t is better fitted by model equation (17). So, neither model 16 nor model 17 gives a perfect fit over a wide range of t. Overall, however, model equation (17), which is based on the liquid superficial velocity, seems to show a slightly better performance than model (16) based on the mean liquid velocity. So at the present stage Eq. (17) is recommended and can be considered as reasonable approximation to the residence time for volumetric introduction for bubble train flow at the capillary number considered here.

A topic which needs further discussion is, in how far the V-RTD evaluated from the DNS data and fitted by Eq. (17) represents the real RTD, based on flux introduction and measurement. We recall that Eq. (17) is based on the two-tanks in series compartment model with a plug flow reactor as first and a stirred vessel as second tank. Interestingly, the RTDs of both the plug flow reactor and the stirred vessel are the same for flux-flux and planar-planar measurement. Namely, for the plug flow reactor the RTD is a delta pulse with zero variance, while the RTD for the stirred tank is derived on the assumption that all the fluid particles are instantaneously perfectly mixed. We thus conclude that model (17) might be a reasonable approximation for the real RTD in bubble train flow.

5. CONCLUSIONS AND OUTLOOK

In this paper we presented an original method for evaluating the liquid phase residence time distribution of bubble train flow using data from direct numerical simulations. The method is a particle method and relies on the uniform introduction of virtual particles in the volume occupied by the liquid phase within a single flow unit cell. The residence time distribution for such a volumetric introduction (V-RTD) is then obtained by statistical evaluation of the time needed by any particle to travel an axial distance equivalent to the length of the flow unit cell. Respective residence time curves have been evaluated from DNS data of bubble train flow in a square mini-channel for different length of the flow unit cell, where the capillary number is in the range $0.2 - 0.25$. The V-RTD curves obtained can well be fitted by a simple exponential function, Eq. (17), which has been developed on the basis of a compartment model consisting of two tanks in series, the first tank being a plug flow reactor and the second being a perfectly stirred vessel. Based on this compartment model it is argued that model (17) is not only a good representation for the V-RTD but also for the real RTD of bubble train flow with flux introduction and measurement.

In future work we will try to extend our particle method from volumetric introduction to a flux introduction method and will investigate the relationship between both RTD curves. Up to now we have only investigated the RTD for a single flow unit cell. In practice, a duct will contain tens or hundreds of unit cells. We will therefore apply our method to multiple lengths of the flow unit cell ($n_{uc} = 2,3, \ldots$) and determine the respective RTD curves. In particular, it will be interesting to check if the RTD for an arbitrary number of n_{uc} can be obtained by convolution of the RTD for a single flow unit cell ($n_{uc} = 1$). Finally, we will investigate if there is any influence of the capillary number on the RTD curve.

REFERENCES

1. T. Boger, A.K. Heibel and C.M. Sorensen, Monolithic catalysts for the chemical industry, *Ind. Eng. Chem. Res.*, vol. 43, pp. 4602-4611, 2004.
2. V. Hessel, S. Hardt and H. Löwe, *Chemical micro process engineering*, Wiley, Weinheim, 2004.
3. J.R. Burns and C. Ramshaw, The intensification of rapid reactions in multiphase systems using slug flow in capillaries, *Lab Chip*, vol. 1, pp. 10-15, 2001.
4. E.B. Nauman, Residence time distributions and micromixing, *Chem. Eng. Commun.*, 8, pp. 53-131, 1981.
5. M. Günther, S. Schneider, J. Wagner, R. Gorges, T. Henkel, M. Kielpinski, J. Albert, R. Bierbaum and J.M. Köhler, Characterisation of residence time and residence time distribution in chip reactors with modular arrangements by integrated optical detection, *Chem. Eng. J.*, vol. 101, pp. 373-378, 2004.
6. A.K. Heibel, P.J.M. Lebens, J.W. Middelhoff, F. Kapteijn and J. Moulijn, Liquid residence time distribution in the film flow monolith reactor, *AICHE J.*, vol. 51, pp. 122-133, 2005.
7. A.A. Yawalkar, R. Sood, M.T. Kreutzer, F. Kapteijn and J.A. Moulijn, Axial mixing in monolith reactors: effect of channel size, *Ind. Eng. Chem. Res.*, vol. 44, pp. 2046-2057, 2005.
8. A. Günther, S.A. Khan, M. Thalmann, F. Trachsel and K.F. Jensen, Transport and reaction in microscale segmented gas-liquid flow, *Lab Chip*, vol. 4, pp. 278-286, 2004.
9. J. Thyn and R. Zitny, Radiotracer applications for the analysis of complex flow structure in industrial apparatuses, *Nucl. Instrum. Meth. B*, vol. 213, pp. 339-347, 2004.
10. C. Castelain, D. Berger, P. Legentilhomme, A. Mokrani and H. Peerhossaini, Experimental and numerical characterisation of mixing in a steady spatially chaotic flow by means of residence time distribution measurements, *Int. J. Heat Mass Transfer*, vol. 43, pp. 3687-3700, 2000.
11. O. Levenspiel, *Chemical Reaction Engineering*, 3rd ed., Wiley, New York, N.Y., 1999.
12. B. Ghidersa, M. Wörner and D.G. Cacuci, Exploring the flow of immiscible fluids in a square vertical mini-channel by direct numerical simulation, *Chem. Eng. J.*, vol. 101, pp. 285-294, 2004.
13. W. Sabisch, M. Wörner, G. Grötzbach, D.G. Cacuci, 3D volume-of-fluid simulation of a wobbling bubble in a gas-liquid system of low Morton number, *4th Int. Conf. Multiph. Flow*, New Orleans, USA, May 27-June 1, 2001.
14. M. Wörner, B. Gidersa, A.F. Shahab, Numerical study of bubble train flow in a square vertical mini-channel: influence of length of the flow unit cell, *5th Int. Conf. Multiph. Flow*, Yokohama, Japan, May 30-June 4, 2004.
15. T.C. Thulasidas, M.A. Abraham and R.L. Cerro, Bubble train flow in capillaries of circular and square cross section, *Chem. Eng. Science*, vol. 50, pp. 183-199, 1995.